Progress In Electromagnetics Research C, Vol. 86, 97–110, 2018

New Stabilization Technique to Prevent Parametric Oscillations in a 35 W C-Band AlGaN/GaN MMIC High Power Amplifier

Mehrdad Gholami[1, 2, *] and Mustapha C. E. Yagoub[1]

Abstract—In this paper, a novel stabilization scheme to prevent parametric oscillations in power amplifiers is presented. Based on a new oscillation detection approach, the inductive degeneration technique was used, for the first time, to successfully stabilize a high-power amplifier and prevent parametric oscillations. A 0.15 µm AlGaN/GaN Microwave Monolithic Integrated Circuit high power amplifier operating at 5.8 GHz with 10% fractional bandwidth was designed and successfully stabilized using this approach. The proposed $(4.7 \times 3.7)\,\mathrm{mm}^2$ three-stage amplifier achieves a saturated output power of 35 W with 29% power added efficiency and a large-signal gain of 26 dB.

1. INTRODUCTION

The use of Microwave Monolithic Integrated Circuit (MMIC) High Power Amplifiers (HPAs) is rapidly growing in radio-communication systems. Lighter and smaller than Travelling-Wave Tube (TWT) amplifiers, MMIC-HPAs are used in Sat-com, RADAR active phased antenna arrays, 5G mobile radio communication, and microwave power transmission, to name a few. They can also be effectively combined to obtain Solid-State Power Amplifiers (SSPAs) [1, 2]. All aforementioned applications operate mainly in the C-band, centred around 5.8 GHz.

AlGaN/GaN transistors are ideal for high power and high efficiency operation due to their high breakdown voltage, high saturated electron drift velocity and high thermal conductivity [3]. GaN HEMTs also offer higher power density and wider bandwidth. Their only current drawback is the relatively low values of the electron/hole mobility, which limit their use in millimetre-wave bands.

Recently, several C-band MMIC-HPAs have been reported as summarized in Table 1. In [4], Qorvo (Triquint) presented two MMIC-HPAs namely, the TGA2578 and the TGA2590, fabricated on 0.25 µm GaN-on-SiC, with 30 W saturated power, 40% power-added efficiency (PAE) and capable of covering most of the C-band [4]. In [5], the latest MMIC generation of HPAs presented by Cree, i.e., the CMPA5585025D, fabricated on 0.25 µm GaN-on-SiC, is suitable for the upper half of the C-band, with 40% PAE and about 40 W saturated power. By using the 0.25 µm GaN HEMT process from United Monolithic Semiconductors (UMS), [6], [7], and [8] have reported 40 W, 40 W and 50 W HPAs, respectively, with more than 40% PAE. MMIC GaN HPAs described in [9–11] have been published without mentioning the producer foundry. MMIC GaN HPA in [10] reported a 52% PAE and 46 dBm saturated power. At the other frequency bands, valuable designs have also been reported such as the one described in [12] and fabricated by Fraunhofer IAF using 0.25 µm AlGaN/GaN HEMTs, which can provide 10 W power and 30% PAE at K-band. A survey of GaN foundries can be found in [13]. The features of the referred HPAs are summarized in Table 1.

Four different kinds of oscillations can occur in microwave power amplifiers: even-mode or small-signal, odd-mode, low-frequency or bias, and parametric [14]. Even-mode and odd-mode oscillations are

Received 26 June 2018, Accepted 6 August 2018, Scheduled 13 August 2018

* Corresponding author: Mehrdad Gholami (mehrdad.gholami@uottawa.ca).

[1] School of Electrical Engineering and Computer Science, University of Ottawa, Ottawa, Canada. [2] Department of Electrical Engineering and Computer Science, University of Calgary, Calgary, Canada.

Table 1. State of the art of C-band GaN-based MMIC-HPAs.

Ref.	Frequency (GHz)	Power (dBm)	PAE (%)	Large Signal Gain (dB)	Size (mm^2)
[4] *	2–6	45	40	22	$6.4 * 5$
[5] *	5.5–9	46	40	22	$3.7 * 4.8$
[6] *	5–5.8	46	41	22	$4.5 * 4$
[7] *	5.4–6.1	46	36	17	$3.8 * 3.9$
[8] *	5.2–6	48	46	20	$4.7 * 3.8$
[9] *	3.6–4	50	64	10	$15.2 * 14.3$
[10] *	5.2–6.8	46	52	22	$3.3 * 3.8$
[11] *	5–6	47.8	40	25	$3.2 * 5.3$
this work **	**5.4–6.1**	**45**	**28**	**26**	$\mathbf{4.7 * 3.7}$

* Measured, ** Simulated

straightforward to be predicted and there exist specific and useful schemes to avoid them. Although low-frequency oscillations cannot be simulated accurately, they can be avoided by using specific schemes and rules. Parametric oscillations may occur when a power amplifier operation switched to the non-linear regime, due to variations of its non-linear internal elements. Such oscillations are not always observable by either the well-known harmonic balance technique or other kinds of simulation methods. So far, in published literature, the only technique to predict the probable parametric oscillations is finding the zero-pole(s) of the amplifier transfer function [15–19]. The real part of all poles must be negative at the desired frequency and power range to avoid parametric oscillations. However, calculating the zero-pole(s) is not convenient and straightforward.

In this paper, a novel and relatively easy method is proposed to predict parametric oscillations. Furthermore, an innovative scheme is proposed to effectively prevent the parametric oscillations with no destroying effects on the overall performance of the amplifier.

To demonstrate the proposed approach, an MMIC-HPA with 150 nm Gate length AlGaN/GaN HEMT technology (GaN150), provided by National Research Council of Canada (NRC), was designed in C-band. GaN150 is offered on silicon carbide wafers of 75 µm thickness. This process has two metal layers, with 50 Ω/sq nichrome resistors and MIM capacitors of 0.19 fF/(µm^2). It allows gold backside and through via thus, making possible the use of microstrip lines. Some electrical features of the process are summarized in Table 2. Note that the time the final HPA layout was ready for fabrication, NRC discontinued the support to this technology. Therefore, only simulation results are presented in Table 1.

Table 2. Major electrical features of the NRC GaN process.

Electrical features	Values
Maximum drain voltage bias	30 V
Maximum power level	7 W/mm
Minimum drain-source breakdown voltage	80 V
Maximum drain current density	1000 mA/mm
Maximum long-term operating drain current density	350 mA/mm
Gate source voltage	-8 V $<$ and $<$ 2 V
Unity gain frequency, f_T	35 GHz
Maximum tolerable current for thick lines	24 mA/µm width
Maximum operating voltage of capacitors	40 V
Maximum breakdown capacitor voltage	180 V

However, the available GaN150 HEMTs are prone to parametric instability. Whereas existing stabilization techniques are not able to stabilize them, the proposed method can carefully detect parametric oscillations and the new stabilization scheme can effectively prevent them. The proposed techniques were demonstrated through the successful stabilization of a 35 W MMIC-HPA designed in C-band.

2. STABILITY ANALYSIS OF POWER AMPLIFIERS

All the above mentioned kinds of oscillations can appear in an HPA. So, a reliable design must take care of all these instabilities. Even-mode oscillations happen when the connected load or source impedances provide a reflection coefficient magnitude bigger than one at the input/output of the transistor. They can occur even without applying an RF signal [20]. In this situation, to achieve an amplifier unconditionally stable for all load/source impedances, a stabilization circuit must be added to the transistor.

Different types of stabilization circuits have been suggested in the literature [14, 20]. However, inserting a lossy circuit at the input of the transistors is usually preferred for optimum performance.

Odd-mode oscillations happen when transistors are put in parallel while the impedances seen from their input/output are not identical. So, the powers delivered to their inputs or obtained from their outputs are unbalanced. These oscillations are more critical in amplifiers using transmission lines. Unwanted coupling between lines is, in fact, one of the main sources of unbalanced impedances at the transistor inputs/outputs [14]. To prevent such oscillations, a small resistor, called isolation resistor, is usually connected between the input and the output of the transistors [21].

Low frequency oscillations are caused by the positive feedback created by the bias supplies, so they cannot be monitored through simulations. They usually occur in amplifiers with large gate FETs at frequency ranges from 10 to 100 MHz. Using a series RC circuit in parallel with de-coupling capacitors at the bias lines can damp these oscillations without any degradation in the overall performance of the amplifier.

Parametric oscillations happen in the large-signal mode when the transistor is driven into its nonlinear region. A power amplifier, perfectly stable under small-signal conditions, may generate parametric oscillations when it is driven close to compression [22]. Such oscillations are due to feedback loops and variations in the transistor's non-linear elements, particularly C_{gs} and C_{gd}, caused by a large RF signal. Parametric oscillations or frequency divisions are generated when the circuit produces a response containing subharmonics of the excitation signal, thus behaving like oscillators. In this situation, subharmonic injection-locking frequency of the fundamental frequency f_{RF} results in a negative resistance at the operating frequency [14].

To detect parametric oscillations, the conventional pole-zero stability analysis is usually performed at the fundamental frequency. This technique has the benefit of being applicable to dc, small-signal, and large-signal stability analyses. The stability analysis is based on determining the poles of a closed-loop transfer function resulting in linearizing the system around a steady state regime [15, 16, 19]. A pole at the fundamental frequency with a positive real part, located in the right half plane (RHP) of the transfer function, reveals the unstable behaviour of the amplifier. If no poles on the RHP are found, the amplifier will be definitely stable. So, the real part of all poles must be monitored when the input power is being increased up to saturation. The calculation of the system poles and zeroes is based on the linearization of the simulated large-signal steady state although it is not straightforward [17, 18]. This linearization is performed by injecting a small-signal current perturbation, at a given frequency, into a node of the circuit and observing the voltage response at this node at that given frequency. A frequency sweep of the perturbation current generator allows to obtain the closed-loop frequency response [23]. In multi-stage microwave power amplifiers, a particular instability generated in one stage may or may not be detected if the probe is connected at a different stage. Therefore, one analysis per stage is required to obtain the complete stability information [23].

Because parametric oscillations are basically caused by the generation of sub-harmonics, it is also possible to calculate and observe the poles' location of the system at half of the input RF-signal fundamental frequency, i.e., at $f_{RF}/2$. The parametric oscillation, being associated to the gain, will decrease and the circuit stability should be improved by introducing series resistors at the gate of any transistor to decrease the gain. Thus, the objective of the stabilization circuit is to decrease the gain

at $f_{RF}/2$ without degrading the overall performance of amplifier at f_{RF}. One way to achieve this, is a parallel RC in series with the gate of the transistor [22, 24]. The resistor should be large enough to make negative the real part of all poles of the transfer function obtained at $f_{RF}/2$ and then, the amplifier will be stabilized. Also, the capacitor must be adjusted to resonate with the resistor at f_{RF}. As a result, the RC circuit is nearly equivalent to a short-circuit at f_{RF} and to a resistor at $f_{RF}/2$ [23]. Instead of a first order parallel RC filter, higher order filters can be also used to achieve better performance and more reliability/stability of the amplifier.

3. PROPOSED INSTABILITY DETECTION AND STABILIZATION TECHNIQUE

At C-band, the gate width of HEMTs can be chosen to be 150 µm or even 200 µm. HEMTs with longer gate will produce more output power but at the expense of reduced gain. However, by careful optimization of the number of gate fingers and gate length, cells of 8×100 µm size were selected for intended HPA to achieve the desired output power and optimum gain with a minimum chip size. DC and S-parameter simulations were performed on the single HEMT cell to find the maximum achievable small-signal stable gain and related bias point. To achieve maximum output voltage sweep and consequently, maximum output power and PAE, the bias point was chosen in class-AB, close to class-B. Hence, selected gate bias voltage was of -3.5 V while the drain voltage value was of 28 V, i.e., close to its maximum allowable value (Table 2). The obtained maximum stable small-signal gain is about 13 dB at 5.8 GHz.

The stability factor, K, and stability measurement, B, have been used to evaluate the small-signal stability behavior of the amplifier for the desired bias values and frequency range.

The single HEMT cell was stabilized (for even-mode) by designing a parallel RC at the input of the gate and a series RL in the bias path of the gate (Fig. 1). However, initial simulations of the single HEMT cell did not converge whereas the HEMT cell was perfectly stabilized for small-signal oscillations (with a minimum values of stability factor $K_{\min} = 1.68$ and stability measurement $B_{\min} = 0.87$) over a very wide frequency range.

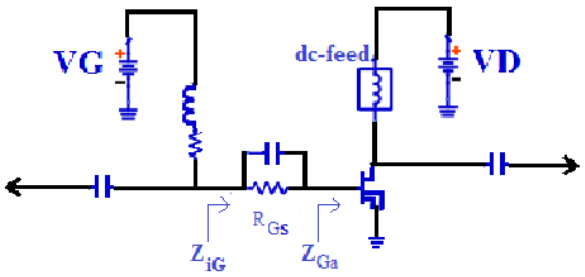

Figure 1. Even-mode (linear) stabilized HEMT single cell.

More investigations showed that the gain of the HEMT cell significantly increases when the input power exceeds the P1-dB compression (corresponding to 22 dBm) thus, demonstrating the parametric oscillations.

As aforementioned, the conventional method to detect parametric oscillations is to calculate the zero-poles of the system transfer function. However, this approach, as well as other reported approaches such as Nyquist criterion [25, 26], floquet analysis [27], and finding the equivalent conversion matrix of the response to small perturbations [28] are not straightforward and requires substantial processing time. Therefore, an efficient and easy method is proposed in this paper to predict such oscillations.

As well known, a circuit is unconditionally stable if the reflection coefficients at its ports are smaller than unity for all passive source and load impedances [20]. Thus, to examine the parametric oscillations, the real part of the input/output impedances of the single HEMT cell must be calculated for a range of input power levels from small-signal to saturation. Note that in a multi-stage amplifier, this process must be performed for each cell as well as for the input/output ports of the amplifier.

The amplifier displayed in Fig. 1 was simulated for all values of the passive output load, and the input impedances Z_{iG} and Z_{Ga} were plotted in the polar coordinate system (Fig. 2) at 5.8 GHz. Fig. 2(a), Fig. 2(b) and Fig. 2(c) show that the real part of the input impedances, Z_{iG} and Z_{Ga}, of Fig. 1 when the input power is 27 dBm (corresponding to P3-dB compression point), 22 dBm (corresponding

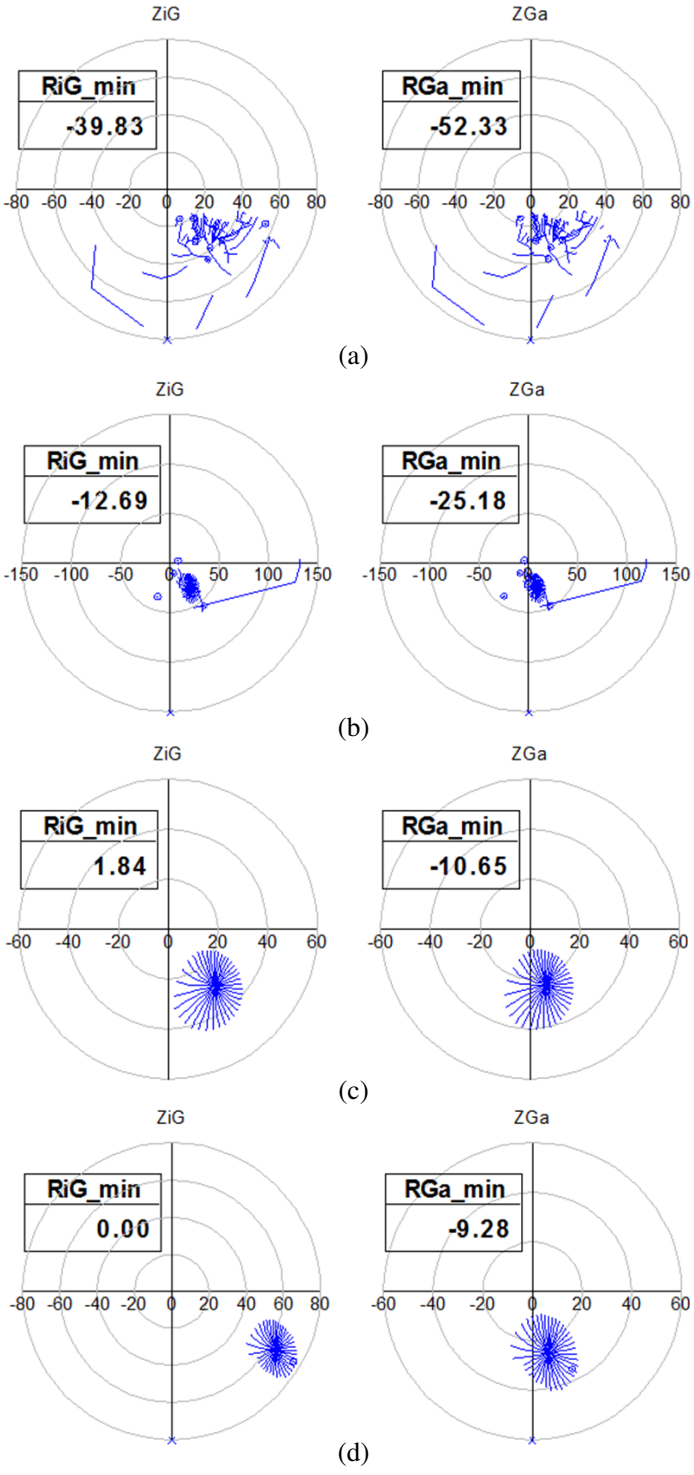

Figure 2. Input impedances, ZiG and ZGa (a) input power is 27 dBm, (b) input power is 22 dBm, (c) input power is 18 dBm and (d) input power is 27 dBm but $RGs = 51\,\Omega$.

to P1-dB), and 18 dBm (linear regime) respectively. Fig. 2(c) demonstrates that the circuit in Fig. 1 is unconditionally stable because the real part of the input impedance (Z_{iG}) for all load values is positive. In fact, the real part of Z_{iG} becomes negative starting from about 20 dB.

To make the real part of Z_{iG} positive and, consequently, stabilize the circuit, the series resistance at the input of the transistor (R_{Gs}) must be increased from 12 Ω to almost 50 Ω (Fig. 2(d)). However, this will lead to an unacceptable decrease of the gain. In fact, the maximum small-signal stable gain will be reduced from 13 dB to 6 dB and the maximum large-signal transducer gain at P3-dB point will be 4.3 dB and about 6 dB at 20 dB back-off. Hence, the performance of the transistor will be degraded so significantly that the transistor will not be suitable for amplification.

Existing stabilizing circuits [29] were examined, but none was successful to stabilize the transistor without exceedingly weakening its performance.

Therefore, a stabilizer scheme was needed to increase the real part of the input impedance of the transistor without degrading its gain. Inductive degeneration technique was found to be the best solution to stabilize the selected AlGaN/GaN HEMT. This technique has been formerly used in low-noise amplifiers (LNA) to match the circuit input impedance to the optimum source impedance, but, to the best of the authors' knowledge, successfully employed for the first time to stabilize a HPA. An inductor at the transistor source increases the real part of its input impedance with no significant degradation of the HEMT performance (Fig. 3).

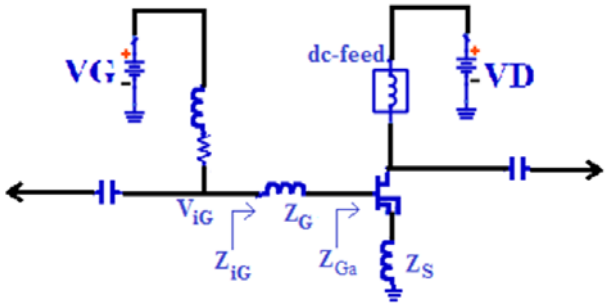

Figure 3. Schematic of the proposed stabilizer circuit.

If the source impedance of the transistor is inductive, then when reflected into the gate, it will become a real resistance. Thus, placing an inductor at the source of the transistor tends to raise the real part of the circuit input impedance [30]. Therefore, it is not only useful for matching purposes but also very helpful for stabilization. As displayed in Fig. 3, an inductor series at the gate as well as a series RL at the gate bias path help preventing the even-mode and parametric oscillations and improving the input matching. The impedance seen at the node V_{iG} (Fig. 3) can be calculated as [30],

$$Z_{iG} = (Z_G + Z_{gs}) + Z_s\,(1 + g_m Z_{gs}) \tag{1}$$

where Z_G represents the impedance of the inductor in the gate, Z_S the impedance of the inductor in the source, Z_{gs} the internal impedance between gate and source, and g_m the output transconductance of the transistor,

$$Z_{iG} \cong jL_G\omega - \frac{j}{\omega C_{gs}} + jL_s\omega\left(1 + g_m\frac{-j}{\omega C_{gs}}\right) \tag{2}$$

$$Z_{iG} \cong \frac{L_s.g_m}{C_{gs}} + j\left(\omega L_G + \omega L_s - \frac{1}{\omega C_{gs}}\right) \tag{3}$$

where Z_G represents the impedance of the inductor in the gate, Z_S the impedance of the inductor in the source, Z_{gs} the internal impedance between gate and source, and g_m the output transconductance of the transistor.

The adverse effect of the proposed scheme is a relatively small reduction of the maximum sweeping drain-source voltage due to the voltage drop across the inductor. Also, using inductive degeneration instead of connecting the transistor's source directly to ground can increase the even-mode

oscillations [31], depending on the value of the inductor. Actually, grounding the transistor's source is always performed by using through vias in MMIC design. These vias produce between 0.05 and 0.1 nH inductance, depending on the technology and operating frequency. So, even-mode oscillations must be examined while including the vias at the transistor's source as well as the proposed degeneration inductor.

In addition, the resonance frequency of the inductor as well as the maximum allowable current through it must be considered. For the selected single HEMT cell, an inductor of about 0.25 nH symmetrically connected to each side of the cell (Fig. 4(a)) can stabilize the transistor perfectly. The maximum small-signal stable gain slightly increased from 13 dB to 14 dB due to removing R_{Gs} at the input of the translator.

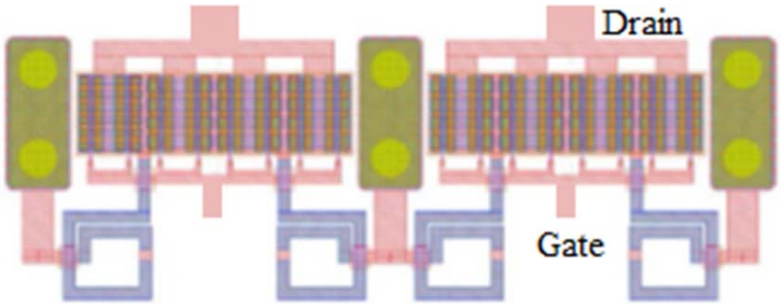

(a)

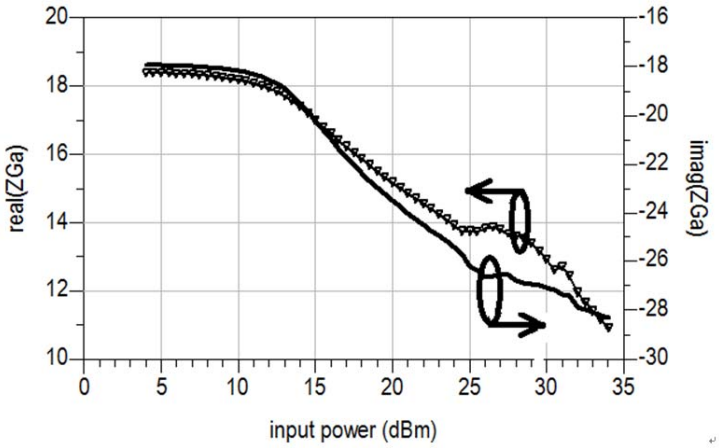

(b)

Figure 4. Stabilized HEMT Cell layout and results. (a) Layout of two 8×100 µm cells with degeneration inductor at the source. (b) Input seen impedance of the HEMT cell, ZGa of Fig. 3 at 5.8 GHz.

Furthermore, simulations showed that drain bias voltages higher than 25 V will increase the risk of parametric oscillations when the single HEMT cells are terminated by a load of value far from its optimum. Thus, drain bias voltage was set to 24 V for more reliability.

The obtained optimum output load of an 8×10 µm single HEMT cell was found to be equal to $(40 + j20)\,\Omega$. The cell can provide 36.5 dBm output power with 9 dB large signal transducer gain and 34% PAE when driven by 27.5 dBm input power (corresponding to P3-dB compression) and terminated by its optimum load. Also, the small-signal transducer gain at 20 dB back-off was 12 dB. Fig. 4(b) shows the real and imaginary parts of the impedance Z_{Ga} versus the input power at 5.8 GHz when the transistor is terminated by its optimum load, demonstrating that the HEMT cell has been fully stabilized. In addition, the real part of Z_{Ga} is positive for the entire desired frequency range. The optimum input impedance of the single HEMT cell was set to $(13 + j27)\,\Omega$ for conjugate matching at the input of the HEMT cell for P3-dB point.

4. DESIGNED MMIC-HPA CONFIGURATION

Based on the above results, a three-stage high power amplifier (HPA) was designed with eight $8\times100\,\mu$m parallel HEMTs at the output stage (stage#1) and two $8\times100\,\mu$m HEMTs at the middle stage (stage#2). For the input stage (stage#3), because a $8\times100\,\mu$m HEMT provides more power than required for stage#2, we selected a $4\times100\,\mu$m HEMT to achieve maximum PAE. The HPA configuration along with a line-up power/gain map is depicted in Fig. 5. It provides 45 dBm output power with a large signal gain of 25 dB. Also, according to this map, all the HEMT cells were derived into the 3-dB compression for an input power of 20 dBm.

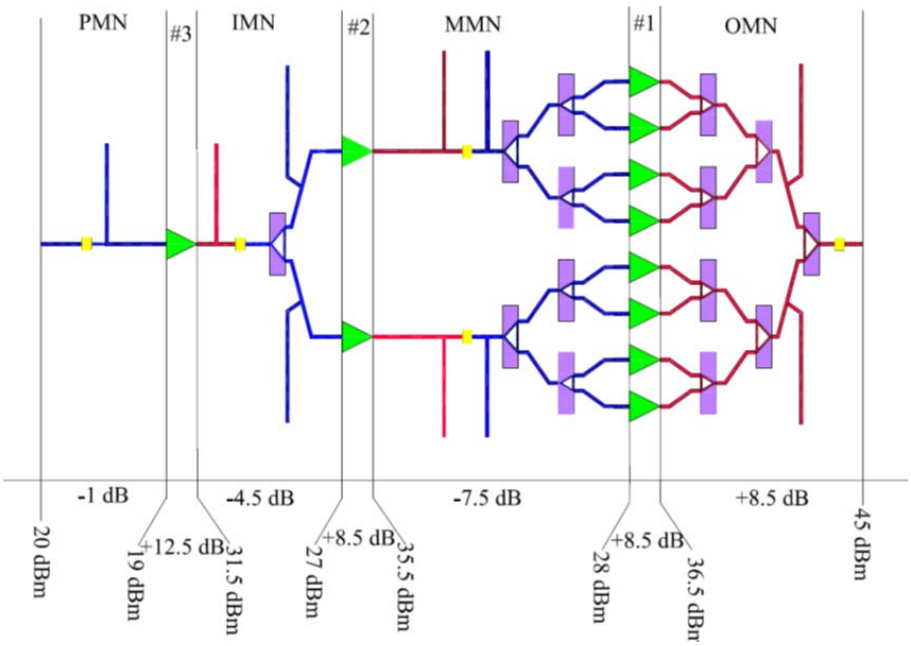

Figure 5. Line-up power/gain map.

Note that in this map, for the matching networks OMN, MMN, IMN, and PMN, 0.5 dB, 1.5 dB, 1.5 dB and 1 dB loss were respectively assumed. The role of the above four matching networks is to combine, split, and transfer the power among the cells properly. Bias circuits were also designed as part of these matching networks. OMN was designed to match the $50\,\Omega$ output port of the HPA to the optimum output load of each cell at Stage#1 as well as to achieve maximum output power. MMN and IMN were designed to match the optimum output load of each cell at Stage#2 and Stage#3 to the conjugated input impedance of the cells in Stage#1 and Stage#2, respectively. PMN is used to match the conjugated input impedance of the cell in Stage#3 to the $50\,\Omega$ input port of the HPA.

A simplified schematic of the HPA circuit is shown in Fig. 6(a). As noted, two series capacitors have been used in OMN to not exceed their maximum operating voltage. The stabilization circuits required to prevent the even-mode, odd-mode, parametric and low frequency (bias) oscillations were included in the matching networks. To achieve higher linearity, a LC series resonator acting as third harmonic suppressor was added to the output matching network.

Meander transmission lines were used in the matching network layouts to obtain compact configurations. However, these lines should not be too close to each other to avoid undesirable coupling. In other side, the transmission lines cannot be drawn very far from of each other to achieve a chip with acceptable size and consequently cost. In fact, the matching networks were not able to provide the exact same impedance for all parallel HEMT cells due to unavoidable coupling between adjacent transmission lines.

Therefore, isolator resistors of about $15\,\Omega$ were added in some specific locations to avoid requiring additional layout area as well as degrading the amplifier performance [32]. These isolator resistors, R_{odd}

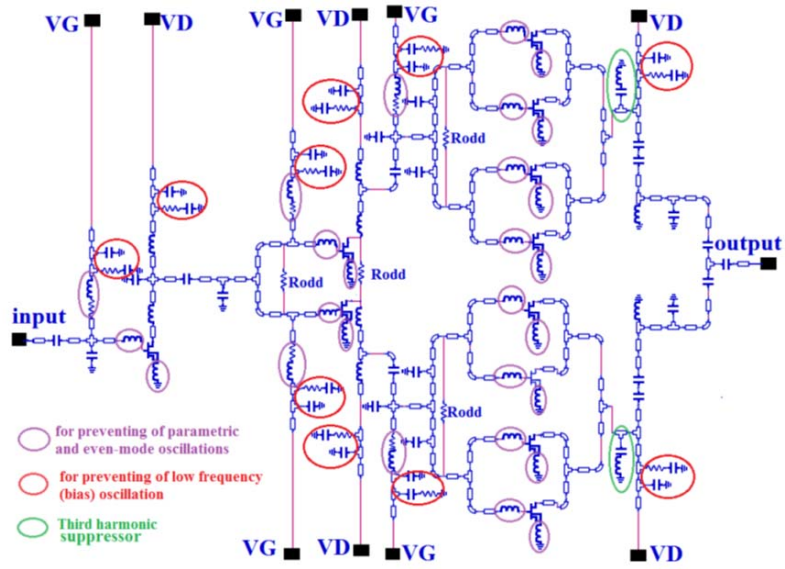

(a)

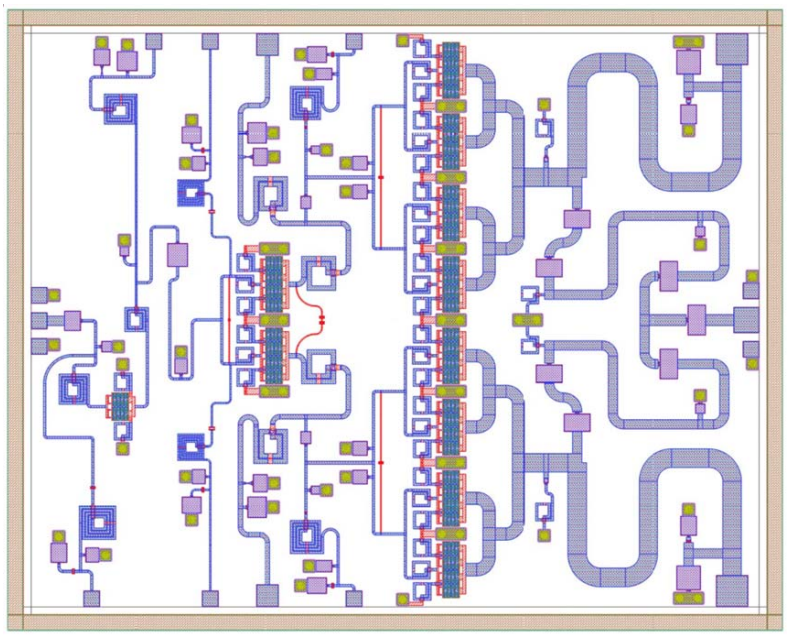

(b)

Figure 6. Designed MMIC-HPA. (a) Simplified circuit schematic of the designed GaN MMIC HPA, (b) HPA Layout (4.7 mm by 3.7 mm).

in Fig. 6(a), could limit the unbalanced power at the gate of each HEMT cell in stage#1 to ±2.5% of maximum available power at the gates. This small amount of unbalanced power is damped in the isolator resistors, so that odd-mode oscillations were totally avoided.

The layouts were simulated in Keysight-ADS Momentum (electromagnetic-EM-simulation) and co-simulation technique was performed to optimize the whole HPA performance (Fig. 6(b)).

Figure 6(b) shows the achieved HPA layout designed in 4.7 mm ∗ 3.7 mm. Two vias were placed between the HEMT cells to create a perfect ground as well as to distribute the heat dissipated by the HEMTs toward the bottom ground plate. All vias, inductors, resistors, and capacitors were also included in the EM simulations of the matching network layouts. The line width of the inductors and feeding tracks were designed carefully to ensure that maximum current densities are not exceeded.

5. RESULTS AND DISCUSSION

Harmonic balance simulations of the optimized HPA coupled to EM simulations of the matching networks' layouts were performed. The obtained real parts of the input/output impedances of the HEMT cells versus the input power of the HPA, up to saturation and for the desired frequency range, are positive, demonstrating the stability of the HPA. The real parts of the impedances at the gate of the cells at each stage of HPA at 5.8 GHz are displayed in Fig. 7, while Table 3 reports the impedances seen at the gate and drain of the cells at 5.8 GHz and for 20 dBm input power.

Note that in this table, "targeted impedances" refer to the impedances used to design the matching networks obtained through load-pull simulations, and "simulated impedances" point out the impedances obtained from the designed HPA.

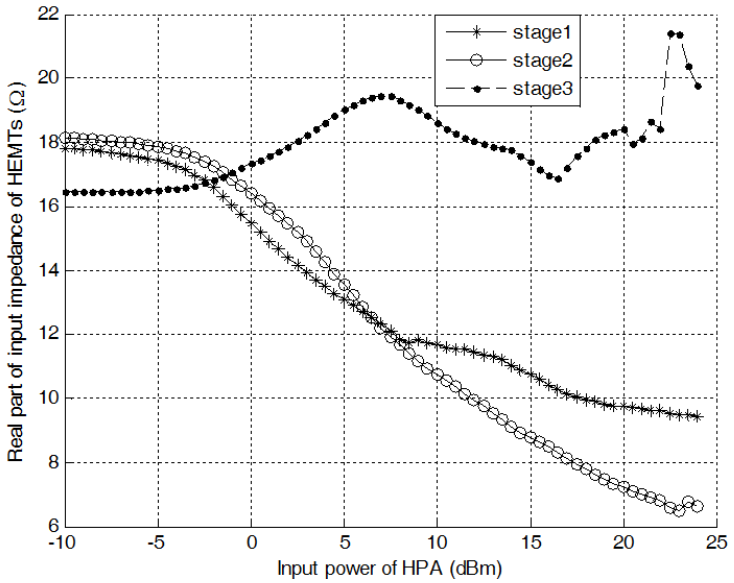

Figure 7. Real parts of the impedances seen at the gate of the cells at each stage, at the fundamental frequency (5.8 GHz).

Table 3. I/O impedances of the HEMT cells at each stage of HPA.

impedance (Ω)	Stage #1	Stage #2	Stage #3
targeted input	$13 - j27$	$13 - j27$	$18 - j65$
simulated input	$9.8 - j26.7$	$7.3 - j25.2$	$18.4 - j60$
targeted output	$40 + j20$	$40 + j20$	$50 + j30$
simulated output	$37.3 + j26.5$	$37.7 + j37$	$56.3 + j12.7$

Figure 8(a) shows the HPA simulations results for an input power sweep at 5.8 GHz. It exhibits 35 dB small-signal transducer gain at 20 dB back-off while the large-signal transducer gain is about 26 dB at P9-dB compression (20 dB input power). The output power is 46 dBm and the PAE 30%, (at P9-dB compression) which completely meet the expectations as depicted in Fig. 5. Fig. 8(b) shows the output power, PAE and transducer gain versus frequency at P9-dB compression point. The HPA can provide more than 45 dBm output power, 29% PAE and 26 dB large signal gain over a 10% fractional bandwidth.

The level of the harmonics is displayed in Fig. 9(a) demonstrating the effect of the third harmonic suppressor. As confirmed in Fig. 9(b) with the total harmonic distortion (THD) parameter, the ratio of the fundamental harmonic power to the sum of all the other harmonic powers is greater than 28 dB, thus

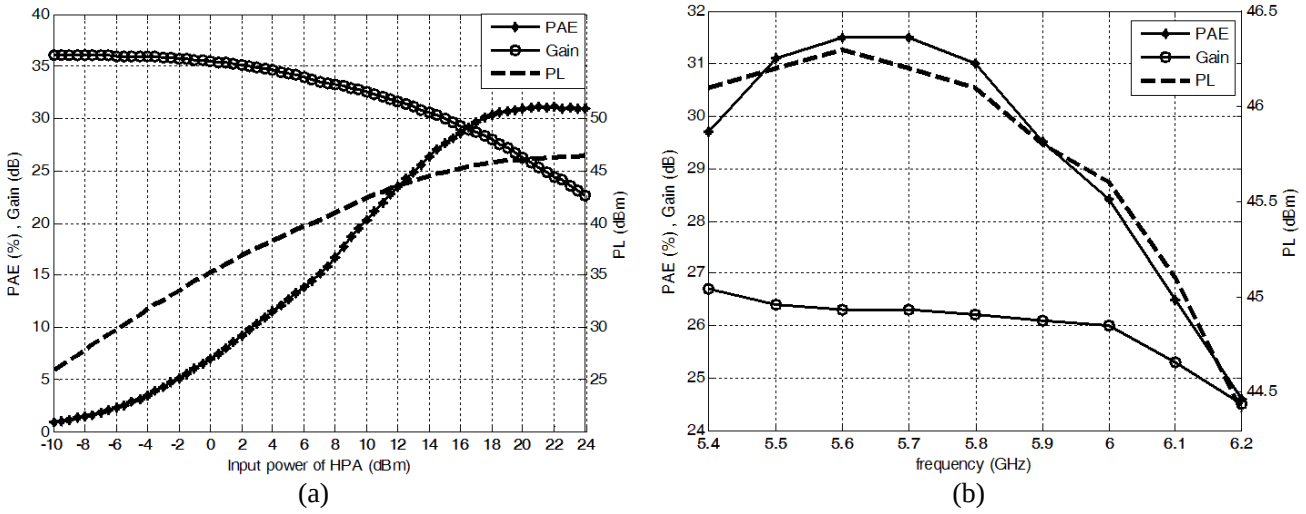

Figure 8. Transducer gain (Gain), PAE and output power (PL). (a) Versus the HPA input power at 5.8 GHz. (b) Versus the frequency at P9-dB compression gain.

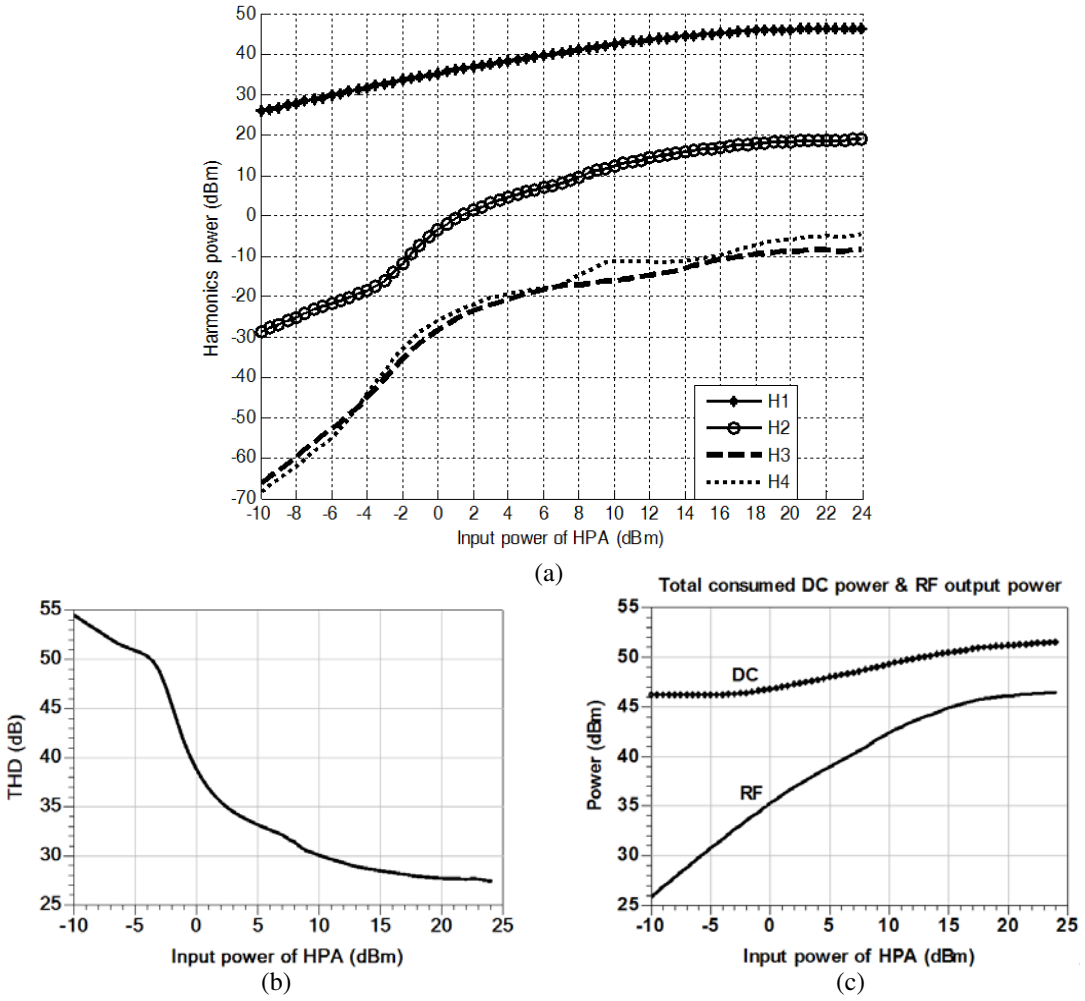

Figure 9. Co-simulation results of whole HPA. (a) Harmonics output power. (b) THD. (c) DC power consumption and RF output power versus input power at 5.8 GHz.

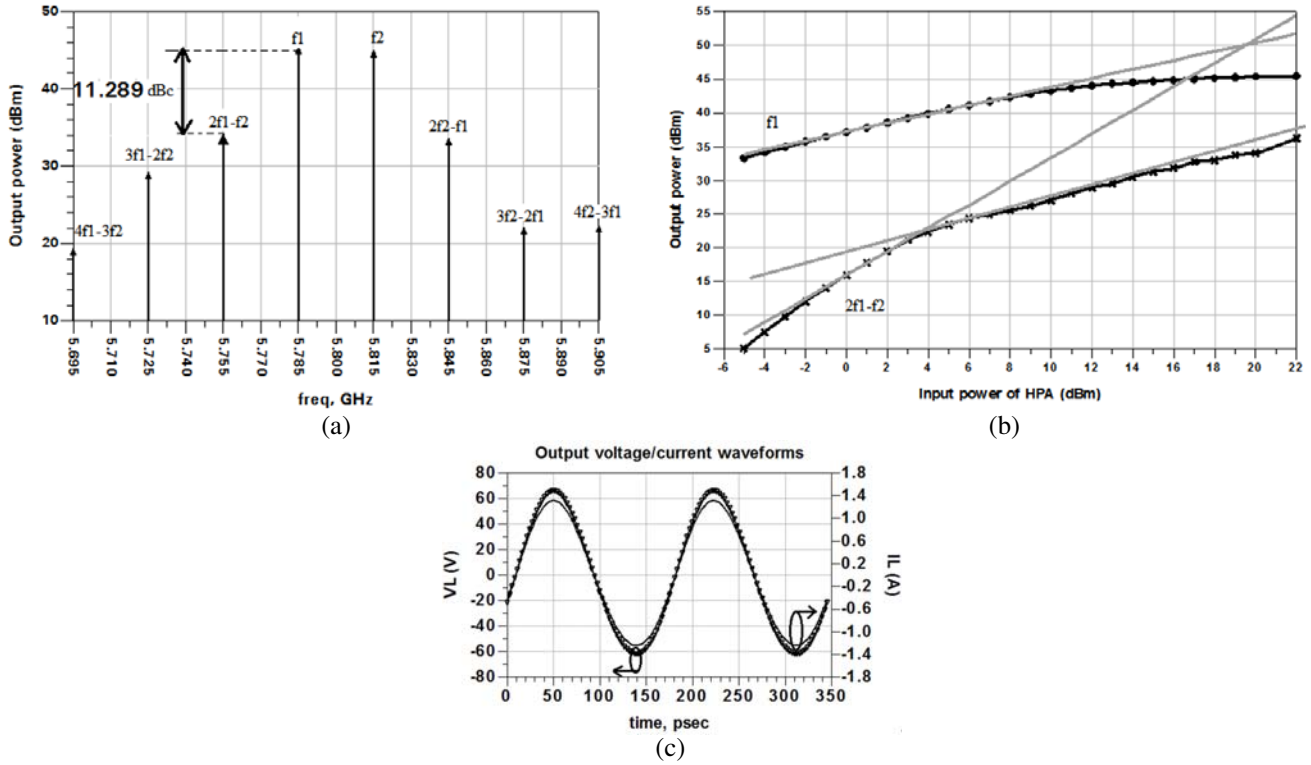

Figure 10. Co-simulation results of whole HPA. (a) Intermodulations and fundamentals power at 20 dBm input power. (b) Fundamental and IM3 power versus input power. (c) Time waveforms of output voltage and current.

demonstrating the high linearity of the HPA. The total consumed DC power has also been compared to the RF output power in Fig. 9(c).

To further confirm the linearity of the HPA, two signals with equal power (20 dBm) and 30 MHz offset were applied to the HPA. The HPA was simulated with four harmonics. Fig. 10(a) shows the output signals at fundamental frequencies, $f_1 = 5.785$ GHz and $f_2 = 5.815$ GHz and their intermodulations. The third order intermodulation (IM3) is about 11.3 dB less than the fundamental signal. Therefore, in multi-channel transmitters, the intermodulations' power is less than the fundamental power by about 7%, thus validating the high linearity of the HPA.

Fig. 10(b) shows the outputs at one of the fundamental frequencies and the third order intermodulation. Let v_i be the voltage amplitude of the two input signals; the output voltage of the fundamental and IM3 of an amplifier of gain G can be written as [30],

$$v_{fund} = Gv_i - \frac{9}{4}bv_i^3 \tag{4}$$

$$v_{IM3} = \frac{3}{4}bv_i^3 \tag{5}$$

where b is a coefficient resulting from the nonlinear characteristics of the HPA and related to its third harmonic magnitude. As shown in Fig. 10(a), because of the third harmonic suppressor, the third harmonic has been reduced significantly, i.e., smaller value of b. According to Eq. (5), the IM3 power will be reduced by using the third harmonic suppressor. As displayed in Fig. 10(b) the IM3 power has a reduction in its slope even when the HPA is still in linear regime (before P1-dB).

For 20 dBm input power, the fundamental output power is about 45.4 dBm, i.e., 0.6 dB smaller than when only one input signal is applied, because of the intermodulations in Eq. (4).

The output voltage and current waveforms are displayed in Fig. 10(c), showing pure equal-phase sin waveforms.

6. CONCLUSIONS

In this paper, a 5.8 GHz three-stage MMIC HPA with 10% fractional bandwidth was designed in the 150 nm AlGaN/GaN HEMT technology. The HEMTs were prone to parametric oscillations and existing stabilization methods were not found efficient to address this issue. To predict the parametric oscillations, instead of determining the zero-poles map, input/output impedances of the HEMTs were considered. Then, for the first time, inductive degeneration was successfully employed to stabilize a HPA and prevent the parametric oscillations. A saturated output power of 35 W, 30% PAE and 26 dB of large-signal gain were achieved in HPA EM co-simulation. Although the HPA was designed in class-AB, its performance is linear and the output signal distortion is very negligible even when the HPA is fully saturated.

REFERENCES

1. Gholami, M., R. E. Amaya, and M.C.E. Yagoub, "Low-loss compact power combiner for solid state power amplifiers with high reliability," *IET, Microw., Antennas & Propag.*, Vol. 10, No. 3, 310–317, 2015.
2. Giofrý, R., P. Colantonio, L. Gonzalez, L. Cabria, and F. De Arriba, "A 300 W complete GaN solid state power amplifier for positioning system satellite payloads," *Microw. Symp. Digest, IEEE MTT-S Int.*, 1–3, 2016
3. Golio, M., *RF and Microwave Semiconductor Handbook*, Ch. 9, CRC, Boca Raton, 2003.
4. http://www.qorvo.com/applications/defense aerospace/radar.
5. http://www.wolfspeed.com/cmpa5585025d.
6. Florian, C., R. Cignani, A. Santarelli, and F. Filicori, "Design of 40-W AlGaN/GaN MMIC high power amplifiers for C-band SAR applications," *IEEE Trans. Microw. Theory and Tech.*, Vol. 61, No. 12, 4492–4504, 2013.
7. Jeong, J. C., D. P. Jang, and I. B. Yom, "A 40 W AlGaN/GaN MMIC high power amplifier for C-band radar applications," *IEEE, European Microwave Conference (EuMC)*, 1126–1129, 2014.
8. Wanum, M. V., A. P. D. Hek, and F. E. V. Vliet, "GaN C-band HPA for phased-array applications," *IEEE Compound Semiconductor Integrated Circuit Symposium (CSICS)*, 1–4, 2013.
9. Miwa, S., Y. Kamo, Y. Kittaka, T. Yamasaki, Y. Tsukahara, T. Tanii, M. Kohno, S. Goto, and A. Shima, "A 67% PAE, 100 W GaN power amplifier with on-chip harmonic tuning circuits for C-band space applications," *Microw. Symp. Digest, IEEE MTT-S Int.*, 1–4, 2011.
10. Noh, Y. S. and I. B. Yom, "Highly integrated C-band GaN high power amplifier MMIC for phased array applications," *IEEE Microw., and Wireless Components Lett.*, Vol. 25, No. 6, 406–408, 2015.
11. Yu, X., H. Sun, Y. Xu, and W. Hong, "C-band 60 W GaN power amplifier MMIC designed with harmonic tuned approach," *Electronics Lett.*, Vol. 52, No. 3, 219–221, 2016.
12. Friesicke, C., P. Feuerschýtz, R. Quay, O. Ambacher, and A. F. Jacob, "A 40 dBm AlGaN/GaN HEMT power amplifier MMIC for SatCom applications at K-band," *Int. Microw. Symposium (IMS), IEEE MTT-S*, 1–4, 2016.
13. Hindle, P., G. Lerude, and R. Mumford, "Get your GaN here: RF GaN foundry survey," *Microwave J.*, Vol. 59, No. 6, 20–34, 2016.
14. Chang, K., V. Nair, and I. J. Bahl, *RF and Microwave Circuit and Component Design for Wireless Systems*, J. Wiley & Sons, 2002.
15. Dellier, S., R. Gourseyrol, G. Soubercaze-Pun, J. M. Collantes, A. Anakabe, and K. Narendra, "Stability analysis of microwave circuits," *IEEE Wireless and Microwave Technology Conf. (WAMICON)*, 1–5, 2012.
16. Dellier, S., L. Mori, J. M. Collantes, A. Anakabe, and C. Campbell, "Analysis of odd-mode parametric instabilities at fundamental frequency in an X-band MMIC power amplifier," *IEEE, Compound Semiconductor Integrated Circuit Symposium (CSICS)*, 1–4, 2016.
17. Jugo, J., J. Portilla, A. Anakabe, A. Suárez, and J. M. Collantes, "Closed-loop stability analysis of microwave amplifiers," *Electronics Lett.*, Vol. 37, No. 4, 226–228, 2001.

18. Collantes, J. M., I. Lizarraga, A. Anakabe, and J. Jugo, "Stability verification of microwave circuits through Floquet multiplier analysis," *IEEE Asia-Pacific Circuits and Systems Conf.*, Vol. 2, 997–1000, 2004.
19. Narendra, K., J. M. Collantes, C. Paoloni, and E. Limiti, "Parametric oscillations in distributed power amplifiers," *Electronics Lett.*, Vol. 45, No. 25, 1325–1326, 2009.
20. Pozar, D. M., *Microwave Engineering*, 4th Edition, 2012.
21. Anakabe, A., J. M. Collantes, J. Portilla, S. Mons, and A. Mallet, "Detecting and avoiding odd-mode parametric oscillations in microwave power amplifiers," *Int. Journal of RF and Microw. Computer-Aided Engineering*, Vol. 15, No. 5, 469–478, 2005.
22. Elad, D., R. Shaulsky, and B. Mezhebovsky, "A novel method for even odd parametric oscillation stability analysis of a microwave power amplifier," *Microw. Symp. Digest, IEEE MTT-S Int.*, 1850–1854, 2006.
23. Anakabe, A., J. M. Collantes, J. Portilla, J. Jugo, A. Mallet, L. Lapierre, and J. P. Fraysse, "Analysis and elimination of parametric oscillations in monolithic power amplifiers," *Microw. Symp. Digest, IEEE MTT-S Int.*, Vol. 3, 2181–2184, 2002.
24. Teeter, D., A. Platzker, and R. Bourque, "A compact network for eliminating parametric oscillations in high power MMIC amplifiers," *Microw. Symp. Digest, IEEE MTT-S Int.*, Vol. 3, 967–970, 1999.
25. Ohtomo, M., "Stability analysis and numerical simulation of multidevice amplifiers," *IEEE Trans. Microw. Theory and Tech.*, Vol. 41, No. 6, 983–991, 1993.
26. Mons, S., J. C. Nallatamby, R. Quéré, P. Savary, and J. Obregon, "A unified approach for the linear and nonlinear stability analysis of microwave circuits using commercially available tools," *IEEE Trans. Microw. Theory and Tech.*, Vol. 47, No. 12, 2403–2409, 1999.
27. Cappelluti, F., F. L. Traversa, F. Bonani, S. D. Guerrieri, and G. Ghione, "Large-signal stability of symmetric multibranch power amplifiers exploiting Floquet analysis," *IEEE Trans. on Microw. Theory and Tech.*, Vol. 61, No. 4, 1580–1587, 2013.
28. Pantoli, L., G. Leuzzi, A. Santarelli, and F. Filicori, "Stability analysis and design criteria of paralleled-device power amplifiers under large-signal regime," *IEEE Trans. Microw. Theory and Tech.*, Vol. 64, No. 5, 1442–1455, 2016.
29. Gonzalez, G., *Microwave Transistor Amplifiers: Analysis and Design*, 2nd Edition, New Jersey, Prentice Hall, 1997.
30. Rogers, J. W. and C. Plett, *Radio Frequency Integrated Circuit Design*, Artech House, 2010.
31. Zomorrodian, V., M. Roberg, T. Nguyen, and W. Gaiewski, "Stability analysis of multi-finger GaN FET cells for high power MMIC design," *Microw. Symp. Digest, IEEE MTT-S Int.*, 1–4, 2016.
32. Ayllon, N., J. M. Collantes, A. Anakabe, G. Soubercaze-Pun, S. Forestier, and D. Langrez, "Joint RF and large-signal stability optimization of MMIC power combining amplifiers," *Int. Journal of Microw. and Wireless Technologies*, Vol. 5, No. 6, 683–688, 2013.